Robust Disaster Impact Assessment With Synthetic Control Modeling Framework and Daily Nighttime Light Time Series Images

Te Mu, Qiming Zheng, and Sylvia Y. He

***Abstract*— Remotely sensed nighttime light (NTL) has been acknowledged as an ideal proxy of the extent and intensity of human activity. One of its main NTL-based applications is to assess disaster impacts; nevertheless, the full potential of NTL-based disaster impact assessment has been largely constrained due to the uncertainties in estimating business-as-usual (BAU) NTL intensity (i.e., the counterfactual condition with no disaster occurrence) and hurdles in isolating the disaster impact from other cocontributing factors of NTL changes. To address these issues, we adopted the synthetic control (SC) modeling framework to construct a robust estimation of BAU NTL with daily NTL images from NASA's Black Marble VIIRS product. We further improved the traditional SC model by optimizing donor selection with the dynamic time warping algorithm (DTW) and incorporating random forest regression to better capture target-donor relationships. Applying our model to 20 severe disasters across geographies, types, magnitudes, and socioeconomic contexts, our model significantly outperformed existing approaches, with an average correlation coefficient of 0.94 against reference and a 0.47% difference of covariates. Besides, our model showed a robust performance in detecting disaster impacts with a low impact intensity and short-term impact duration, which were largely under-detected by existing approaches. The resulting disaster impact assessment metrics, including impact duration, impact intensity, and impact severity, provided further insights into the substantial heterogeneity in disaster coping capability and socioeconomic resilience across regions. Our proposed model holds a broad significance in supporting not only strategic and effective disaster relief but also achieving ambitious climate resilience and sustainability goals.**

***Index Terms*— Black marble product, disasters, nighttime light (NTL), synthetic control (SC), time series analysis.**

I. Introduction

REMOTELY sensed nighttime light (NTL) has been acknowledged as one of the most widely used data to quantify human activity [1], [2]. It complements conventional "daytime" remote sensing imagery by offering a unique understanding of urbanization and socioeconomic changes [3]. Over the past three decades, advances in sensor platforms, image processing algorithms, and analysis-ready data products have brought revolutionary improvements in NTL images in terms of quality, temporal span and frequency, spatial resolution, and spectral properties [4], [5], [6], [7]. These advances have not only strengthened existing NTL-based applications, particularly with finer spatiotemporal details and expanded temporal coverage but also drawn forth new NTL-based applications [2], [8].

In addition to mapping urban areas [9], socioeconomic variables [10], [11], and light pollution [12], [13], another main thread of NTL-based applications is disaster impact assessment, including natural disasters (e.g., hurricanes, earthquakes, and floods) and man-made disasters (e.g., regional conflicts) [14], [15], [16], [17], [18]. The detected NTL intensity is used as a proxy of human activity intensity, allowing researchers to compare NTL images before and after the disaster to quantify the impact intensity of the disaster, estimate the recovery duration, and map their spatial patterns. These metrics are crucial for a quantitative and comprehensive understanding of disaster impacts and informing effective post-disaster recovery strategies, which thereby are essential levers of achieving ambitious risk reduction and climate adaptation goals, such as the Sendai Framework for Risk Reduction 2015–2030 [19] and Sustainable Development Goals (Target 11.5-make human settlement resilient) [20].

In spite of the merits of NTL-based disaster assessment, its full potential has been constrained by the following issues. First, while daily NTL data has been available since 2018, most studies are built on monthly and yearly composite data to avoid high temporal variation and prevailing data gaps of daily NTL data [21]. Besides, studies often rely on oversimplified comparisons using only two NTL images at two timeslots before and after the disaster [22], [23]. These disaster assessment approaches not only underuse the abundant temporal information of daily NTL images but merely provide a sketchy and arbitrary snapshot of disaster impacts. Second, it lacks an effective approach to estimating business-as-usual (BAU) NTL intensity during the post-disaster period. In comparison with the observed NTL intensity, BAU NTL intensity is an unobservable counterfactual that assumes no disasters occurred [24]. Accurate and robust estimation of BAU NTL intensity is key to disaster impact assessment because it is

Received 1 September 2024; revised 13 November 2024; accepted 3 December 2024. Date of publication 9 December 2024; date of current version 31 December 2024. This work was supported in part by The Chinese University of Hong Kong under Grant 4937239, in part by the General Research Fund of the Research Grants Council of Hong Kong under Project CUHK 15204824, and in part by Hong Kong Polytechnic University under Grant P0044791. *(Corresponding author: Qiming Zheng.)*

Te Mu and Qiming Zheng were with the Department of Land Surveying and Geo-Informatics, Hong Kong Polytechnic University, Hong Kong, SAR, China. They are now with the Department of Geography and Resource Management, The Chinese University of Hong Kong, Hong Kong, SAR, China (e-mail: mateomu@link.cuhk.edu.hk; qmzheng@cuhk.edu.hk).

Sylvia Y. He is with the Department of Geography and Resource Management, The Chinese University of Hong Kong, Hong Kong, SAR, China (e-mail: sylviahe@cuhk.edu.hk).

This article has supplementary downloadable material available at https://doi.org/10.1109/TGRS.2024.3512549, provided by the authors.

Digital Object Identifier 10.1109/TGRS.2024.3512549

Fig. 1. Locations and types of the selected disasters and their spatial scale of the corresponding affected areas (i.e., country scale or state/county scale).

one of the fundamental components of deriving assessment metrics. For example, the intensity of disaster impact is often calculated by comparing BAU NTL with the observed NTL, while the recovery duration is estimated by the time lapse between the disaster event and the observed post-disaster NTL recovers to BAU level. Most existing studies determine the BAU NTL intensity with the average NTL intensity of a certain pre-disaster period (e.g., 30-day or 180-day) [23], [25]. Others fit the pre-disaster NTL time series with a predefined model (e.g., simple linear, logistic, and polynomial models) and extrapolate the fit model to estimate BAU NTL intensity during the post-disaster period [24], [26]. Identifying a one-size-fits-all temporal pattern is, nevertheless, barely possible as the NTL pattern is highly complicated and combined with the understudied and intertwined uncertainties from ephemeral and multisource noise signals [27], [28]. Last, studies tend to overlook the NTL changes caused by factors other than disasters. Existing studies often assume that the detected NTL changes are solely attributed to disasters [29], while NTL changes can also be the other consequences, such as regional urbanization and long-term socioeconomic recession [30]. The abovementioned limitations have given rise to large uncertainties and challenges in effective disaster impact assessment with NTL data.

To address these challenges, we proposed a new approach to construct robust BAU NTL and to improve disaster impact assessment with daily NTL time series images and the synthetic control (SC) modeling framework. Specifically, we 1) improved the traditional SC model by developing a donor selection optimization algorithm and incorporating random forest regression to better capture the target-donor relationship and 2) applied our proposed model to 20 disasters across different disaster types, scales, and geographies, together with a series of comparisons, to investigate the performance and merits of our model.

II. Study Area and Datasets

A. Study Area

We selected 20 disaster cases, including 17 natural disasters (e.g., earthquakes, floods, hurricanes) and three anthropogenic disasters (i.e., wars) (Fig. 1), due to their frequent occurrence worldwide and significant socioeconomic impacts. These cases were chosen to ensure a broad representation of disaster types, geographic locations, socioeconomic contexts, and spatial scales of affected areas (e.g., national or regional levels), in order to explore varying patterns of impact and recovery across different regions. The natural disaster cases were obtained from the International Disaster Database, which provides comprehensive details such as start date, affected regions, and total fatalities [31]. Only disasters occurring after 2012 were considered because of the availability of VIIRS NTL data. We selected 17 natural disasters based on their substantial economic impact on the primary affected regions. Each disaster is identified by its location and type, such as Puerto Rico Hurricane Maria or Kochi Flood (Fig. 1).

B. Datasets

1) NTL Data: Our study used the moonlight and atmosphere-corrected NTL images from NASA's Black Marble product suite (VNP46A2) of Suomi NPP VIIRS Day/Night Band data [32]. VNP46A2 is one of the most high-quality NTL

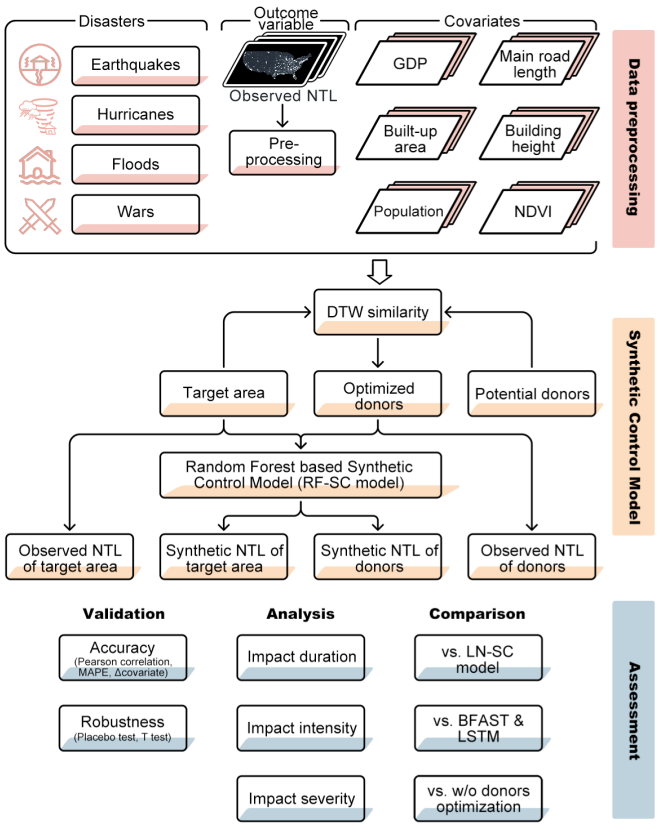

Fig. 2. Flowchart of our proposed framework.

image products that have undergone a series of corrections to screen out noises from snow, lunar, aerosol, and other ephemeral light [32]. VNP46A2 has provided 15 arc-s daily VIIRS NTL data since 2012, comprising seven image layers of NTL radiance and quality control information [27]. In our study, we used the lunar BRDF-corrected DNB NTL radiance layer and the mandatory quality flag layer to screen out low-quality observations [33]. We obtained all the daily VNP46A2 data from Google Earth Engine from 180 days before to 179 days after the occurrence of each disaster [34].

2) Other Datasets: In addition to NTL time series images, we obtained the following data as the input covariates of the SC model to characterize the socioeconomic and environmental status of target areas (disaster-affected areas) and donor areas (disaster-unaffected areas): total population size, average building height, total built-up area, mean normalized difference vegetation index (NDVI), gross domestic product (GDP), and total main road length (Table S1).

III. Methods

Our proposed methodological framework comprises three parts: 1) data preprocessing; 2) developing an improved SC-based model to construct robust BAU NTL time series; and 3) evaluating model performance from multiple aspects and applying our proposed model to assess the impacts of the selected disasters (Fig. 2). Below are the details of our proposed methods.

A. NTL Data Preprocessing

We identified and excluded low-quality observations for each pixel with the mandatory quality flag layer of VNP46A2. We then used a second-order polynomial interpolation to replace these low-quality observations. To screen out signals incurred by ephemeral light sources and background noises, we masked out the pixels with a median NTL intensity below the 5th percentile of each study area during the pre-disaster period [27]. Finally, we calculated the total NTL intensity for each study area, including both target and donor regions, on a daily basis across the entire pre-disaster and post-disaster periods.

B. Improved SC Model

The SC model is a quasi-experimental technique to identify and quantify the effect of an intervention on the variable of interest (termed outcome variable) [35]. It does not rely on a predefined pattern of outcome variables and is robust against other concurrent influencing factors and unknown noises [36]. The SC model constructs a synthetic target area and synthetic outcome variable under a counterfactual condition where no intervention has occurred [37] (Fig. 3). This synthetic target area is constructed by a modeled relationship between the target area and control areas (termed donors), which have not been exposed to the intervention but share similar covariates with the target area. The synthetic outcome variable for the target area is then estimated by applying the modeled relationship to the outcome variable of donors. Measuring the resulting difference between the observed and synthetic outcome variables during the postintervention period (termed treatment effect) helps to determine whether the intervention has caused a significant impact and quantifies the impacts.

Building on these strengths, we developed an SC-based model to assess the disaster impact with daily NTL images while controlling coinfluencing and underexplained factors of NTL changes. Specifically, we adopted the SC model concept to construct a synthetic target area and used the resulting synthetic NTL time series as the BAU NTL under the counterfactual no-disaster condition. For consistency and clarity, we used "synthetic NTL" to represent both "synthetic NTL" and "BAU NTL" in the subsequent content. The difference between synthetic NTL and observed NTL (i.e., treatment effect) was then calculated to measure the impact of each disaster on human activities (Fig. 3).

Constructing robust synthetic NTL intensity time series, however, depends heavily on the resemblance of selected donors to the target area and the accuracy of the modeled relationship between the target area and donors. Most existing SC-based studies selected the donors via a trial-and-error process [38], [39]. Without an objective and quantitative selection protocol, donor selection is extremely time-consuming and, more importantly, risks misleading results due to inappropriate donor selections [40]. The linear regression model was mainly used to capture the relationship between target area and donors. Although it is effective for linear pattern fitting, it is inadequate for handling remote sensing data with complicated patterns like NTL data [41] and vulnerable to

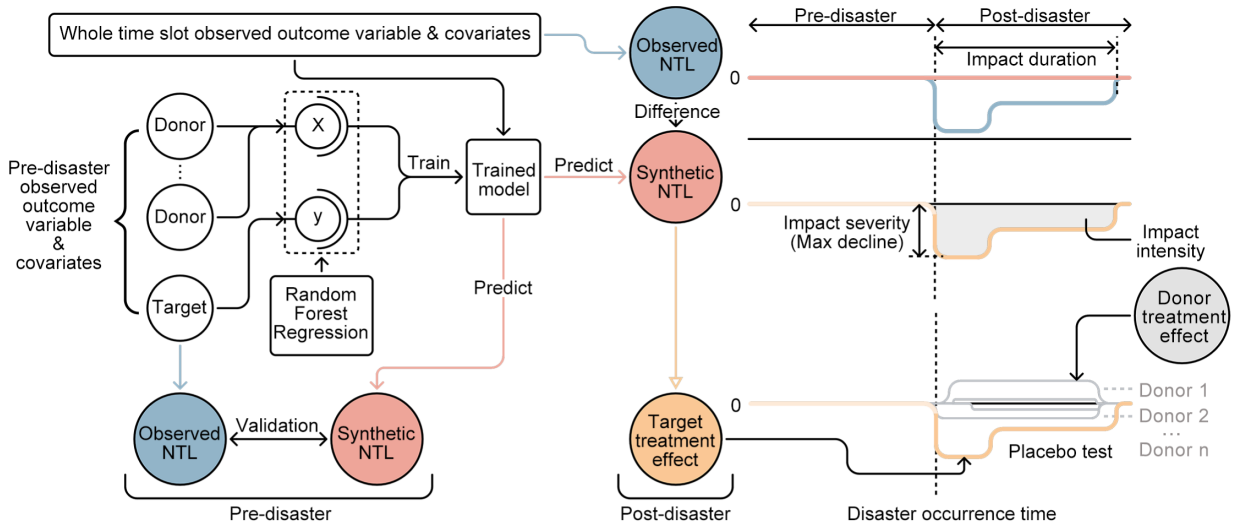

Fig. 3. Conceptual diagram of SC model.

underfitting [42]. To address these challenges, we proposed an improved SC model (named RF-SC model) that incorporates a donor selection optimization approach and employs a random forest regression model for target-donor relationship modeling.

1) Donor Pool Selection Optimization: We applied the dynamic time warping algorithm (DTW) to quantify the similarity between the target area and donors, providing a quantitative basis for donor pool selection [43]. A shorter cumulative DTW distance indicates greater similarity between these data (see Supplementary Text 1 for further details). For each disaster, following the previous study [40], we selected 20 regions geographically closest to the target area, unaffected by the disaster and at the same administrative level as the potential donors. These potential donors covered an area similar in size to the target area. Then, we use the DTW method to select the optimal donors from the pool of potential donors. To achieve this, we selected population, built-up area, and GDP to describe the characteristics of the target area and potential donors and calculated their respective cumulative DTW distances. Then, we normalized each cumulative DTW distance for all potential donors, resulting in the normalized population distance (S_{POP}), built-up area distance (S_{BA}), and GDP distance (S_{GDP}). (1) A smaller S_{Total} indicates a higher similarity between the characteristics of a donor and the target area. We selected the 15 regions with the smallest S_{Total} as the final optimized donors

$$S_{\mathrm{total}} = S_{\mathrm{POP}} + S_{\mathrm{BA}} + S_{\mathrm{GDP}} \tag{1}$$

where S_{POP}, S_{BA}, and S_{GDP} are the normalized cumulative DTW distance of population, build-up area, and GDP.

2) Random Forest-Based SC Model: We replaced the commonly used linear regression model (LN-SC model) with a random forest regression model to better capture the nonlinear relationship between the target area and donors, as well as reduce the noise and overfitting [44], [45]. We trained a random forest regression model using the pre-disaster outcome variable and covariates of the target area and the corresponding optimized donors. The trained model was then applied to construct a synthetic NTL time series (i.e., outcome variable) and the covariates throughout the entire study period, and the treatment effect was calculated to quantify the disaster impact.

C. Model Performance Evaluations

1) RF-SC Model Performance Evaluations: We applied the RF-SC model to each selected disaster and evaluated its performance and robustness. First, we examined how well the synthetic target area and synthetic NTL time series were constructed by calculating the percentage difference between the synthetic and observed covariates, as well as the Pearson correlation coefficient between the synthetic and observed NTL during the pre-disaster period. A smaller percentage difference and higher correlation coefficient indicate better performance of the RF-SC model in constructing a synthetic target area and synthetic NTL, respectively.

Second, two tests were performed to examine the robustness of the detected treatment effect.

1) We compared the magnitude of the treatment effect and modeling error (i.e., the difference between synthetic and observed NTL in the pre-disaster period) to determine whether the treatment effect was due to the disaster or modeling error;

2) To ensure the treatment effect was solely attributable to the studied disaster rather than other concurrent events, we performed a placebo test, an approach widely used in SC studies [40] (Fig. 3). The placebo test selected one of the 15 donors as the pseudo "target area," constructed a synthetic NTL time series of the selected donor using the remaining 14 donors, and calculated its treatment effect. We repeated this procedure to calculate the treatment effect of each of the 15 donors. Since donors were not exposed to disasters, their treatment effects should theoretically be zero and significantly differ from the treatment effect of their corresponding target area. If not, it suggests that the detected treatment effect is, at least partially, caused by other concurrent events rather than disaster.

2) Comparisons With Different Models: To further illustrate the merits of our proposed method, we compared it with other

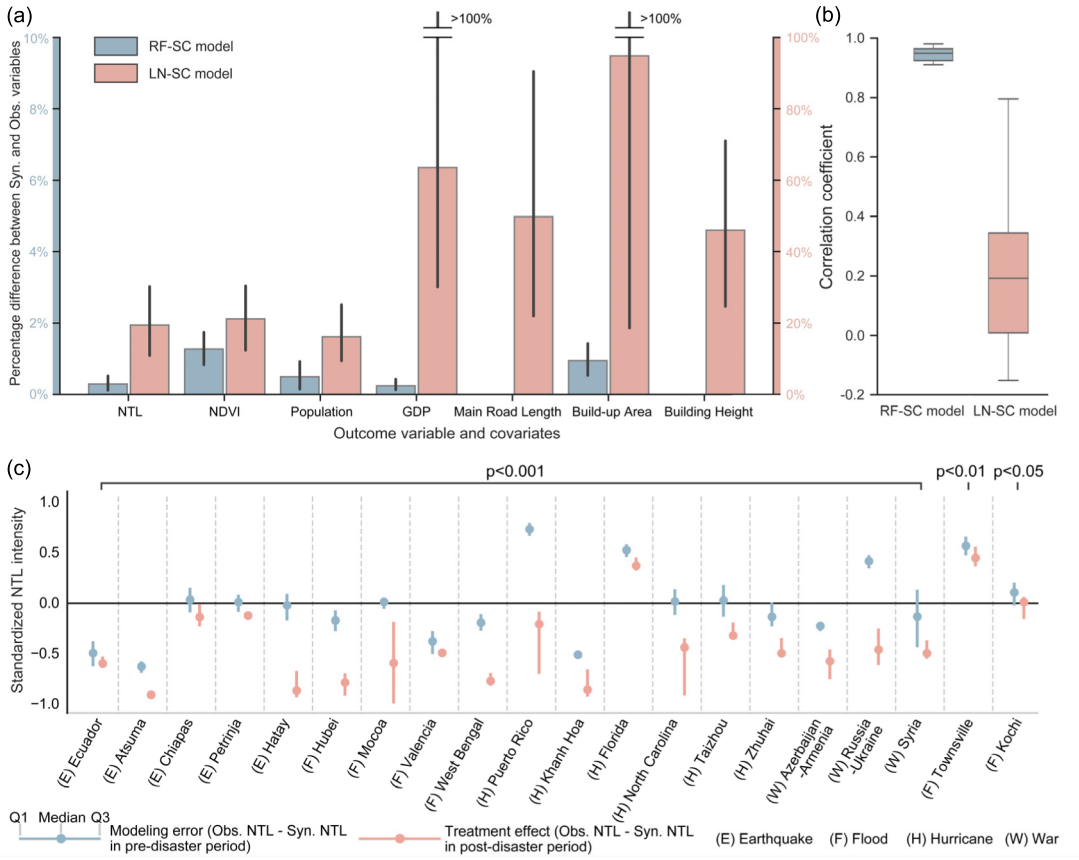

Fig. 4. Performance evaluation of our proposed RF-SC model. (a) Mean and standard deviation (error bar) of the percentage difference between the synthetic and observed outcome variable and covariates of all studied disasters, where the blue and red bars indicate the results obtained from the LN-SC model and RF-SC model, respectively. (b) Correlation coefficient between synthetic NTL and observed NTL that were obtained from the LN-SC model and RF-SC model of all studied disasters ($n = 20$). (c) Magnitude of standardized modeling error and treatment effect. E, F, H, and W represent earthquakes, floods, hurricanes, and wars, respectively.

commonly used approaches. First, we applied the proposed RF-SC model and the traditional LN-SC model to all the studied disasters and compared their performance from the perspective of synthetic NTL estimation and treatment effect detection (see Supplementary Text 2 for further details). Second, to investigate the methodological merit of the SC-based approach, we compared our RF-SC model with two other time series analysis models that have been applied in other NTL-based disaster impact analyses, i.e., the breaks for the additive season and trend model (BFAST) [46] and the long short term memory network (LSTM) [47], [48] (see Supplementary Text 3 for further details).

D. Analysis and Disaster Impact Assessment

With a detailed proof-of-concept of our RF-SC model, we assessed the impacts of each selected disaster by developing the following impact assessment metrics.

1) *Impact Duration:* The time-lapse from the first day of the disaster to the day before the first time the observed NTL returned to BAU level of NTL intensity (i.e., synthetic NTL). We applied a 13-day median filter to smooth the treatment effect curve to reduce the high temporal variation and prevailing fluctuation in NTL data and avoid underestimating the impact duration (Fig. 3).

2) *Impact Intensity:* The sum of the percentage difference between synthetic NTL and observed NTL from the occurrence of the event to the day of recovery (2). It was calculated as follows:

$$I_n = \sum_{t=1}^{T} \frac{|\text{Obs}_t - \text{Syn}_t|}{\text{Syn}_t} * 100 \tag{2}$$

where I_n represents the impact intensity of target event n. Syn_t and Obs_t are the synthetic and observed NTL of the tth day after the disaster. T is the impact duration.

3) *Impact Severity:* The maximum percentage decline in observed NTL intensity relative to the synthetic NTL intensity during the post-disaster period.

IV. Results

A. Performance of RF-SC Model

Our evaluation demonstrated that our proposed RF-SC model can robustly construct synthetic target areas with the donors, as evidenced by extremely small percentage differences between observed covariates and synthetic covariates of target areas [Fig. 4(a)]. Across all the studied disasters, the average percentage difference of each covariate was 0.47% ± 0.45% (mean ± std), with the highest difference observed in generating synthetic NDVI (1.27% ± 1.04%).

These resulting percentage differences of covariates were well below the threshold typically considered robust in most SC-based studies [49]. Additionally, our RF-SC model achieved a high correlation coefficient (0.94 ± 0.02) between synthetic and observed NTL time series during the pre-disaster period, ranging from 0.91 (Petrinja Earthquake) to 0.98 (Azerbaijan-Armenia War) (Table S2). This marks a significant improvement over the traditional LN-SC model (0.29 ± 0.2) in capturing NTL change patterns [Fig. 4(b)]. In fact, applying the traditional LN-SC would lead to a less satisfactory and unstable performance, where 18 out of 20 studied disasters exhibited a correlation coefficient below 0.5, such as the Ecuador Earthquake (0.20), the Hubei Flood (0.18), and the Russia-Ukraine War (0.30). Last, the treatment effects detected in all the studied disasters were statistically larger than the modeling error [$p < 0.05$; Fig. 4(c)]. This allows us to reject the null hypothesis that the disaster impact detected by our RF-SC model was a consequence of modeling error. These findings underscore the capabilities of our RF-SC model in constructing high-quality synthetic NTL time series for disaster impact assessment.

B. Disaster Impact Assessments

With the proof-of-concept above, we applied the RF-SC model to assess the impacts of all studied disasters by the resulting synthetic and observed NTL time series, treatment effect curves, placebo tests, and the disaster assessment metrics (i.e., intensity, duration, and severity). Firstly, the placebo tests confirmed that the treatment effects observed in each disaster's target area were significantly larger than those in the placebo cases ($p < 0.05$; Figs. 5 and S1). It indicates that the observed disaster impacts on human activities in the target areas were solely attributable to the disasters rather than to other concurrent factors affecting the region.

More importantly, our assessments illustrated that the RF-SC model effectively detected and tracked disaster impacts across various conditions. Some disasters, such as the West Bengal Flood (166 days), the Russia-Ukraine War (over 180 days), and the Azerbaijan-Armenia War (over 180 days), had notably long-lasting effects. For example, Hurricane Maria, one of the most severe hurricanes to hit Puerto Rico, resulted in an incomplete and slow recovery, with NTL intensity not returning to pre-disaster levels even six months after landfall [Fig. 5(a)]. This finding aligns with previous reports and studies on the posthurricane recovery of Hurricane Maria [50], [51]. In addition to disasters with a long-lasting impact, our model also performed well in detecting shorter-term disaster impacts, such as those from Hatay Earthquake (16 days; Fig. S1g), Kochi Flood (12 days; Fig. S1f), and Ecuador Earthquake (13 days; Fig. S1b). This reflects a key advantage of our RF-SC model, as detecting the impact of short-term disasters, especially earthquakes, has been challenging in previous NTL-based studies [52], [53].

The resulting treatment effect curve allowed us to better understand how disaster impact unfolded over time. Taking the Russia-Ukraine war as an example, the pattern of treatment effect was closely related to the war's progress. It showed a decline-rebound-decline pattern since the war outbreak on February 24, 2022 [Fig. 5(d)]. After the Russian occupation of the Kherson Oblast in Ukraine on March 2, 2022, there was a significant decline in NTL intensity in the region, down to 22% of the BAU level. Subsequently, NTL intensity continued to decline, then experienced a partial recovery about 60 days after the war outbreak. The recovery could be attributed to a stalemate between the conflict parties during this period, the return of Ukrainian refugees, and reconstruction efforts [54]. Soon after, however, Ukraine launched a counter-offensive, taking control of parts of Donetsk and imposing martial law, while Russia carried out air strikes on electrical infrastructure within Ukraine [54]. These actions resulted in a further decrease in NTL intensity down to 40% of the BAU level.

The disaster assessment metrics provided further insights into the substantial heterogeneity in disaster impacts, disaster coping capability, and socioeconomic resilience (Table I). Disasters, such as the Ecuador Earthquake (0.12), the Kochi Flood (0.45), and the Valencia Flood (0.44), had relatively minor impacts on the target areas, whereas the impacts of Russia-Ukraine War (75.96), Puerto Rico Hurricane Maria (70.23), and Syria Civil War (55.55) were rather substantial. Notably, West Bengal Cyclone Amphan, in spite of having a medium-level impact severity (27.50%), had a prolonged impact duration (166 days), with only 18 out of 166 days (11%) experiencing an NTL decrease exceeding 25% of the BAU level (Table S3). In contrast, while Mocoa experienced a higher impact severity (31.67%) than West Bengal, it recovered to its BAU level in just 57 days, approximately one-third (38%) of the time taken by West Bengal.

C. Model Performance Comparisons

1) RF-SC Model Versus LN-SC Model: The RF-SC model demonstrated superior performance in generating accurate synthetic NTL time series, resulting in more reliable disaster impact detection and assessment compared to the traditional LN-SC model (Fig. 6). Our analysis showed that the LN-SC model tended to risk creating unreliable synthetic NTL and consequently resulted in a false treatment effect, albeit with the optimized donors (Table S2). Taking Florida Hurricane Irma as an example, the synthetic NTL generated by the RF-SC model exhibited good accordance with the observed NTL during the pre-disaster period (correlation coefficient = 0.94), thereby successfully detecting its impact, although the impact intensity was relatively low [Fig. 6(b)]. In contrast, the unsatisfactory performance of the LN-SC model in estimating synthetic NTL (correlation coefficient = 0.29) led to a huge gap between synthetic and observed NTL and failed to detect the impact of Hurricane Irma [Fig. 6(a)]. Similarly, in the case of the Petrinja Earthquake, its short-term and less intense impact was buried in the modeling error of the LN-SC model [Fig. 6(c)]. In fact, the LN-SC model detected the impact of only 10 out of the 20 studied disasters (Fig. S2). These findings highlight that the RF-SC model outperforms the LN-SC model, which is less suitable for constructing robust NTL for disaster detection.

2) SC-Based Approach Versus Other Time Series Models: The advantage of the SC-based approach in detecting

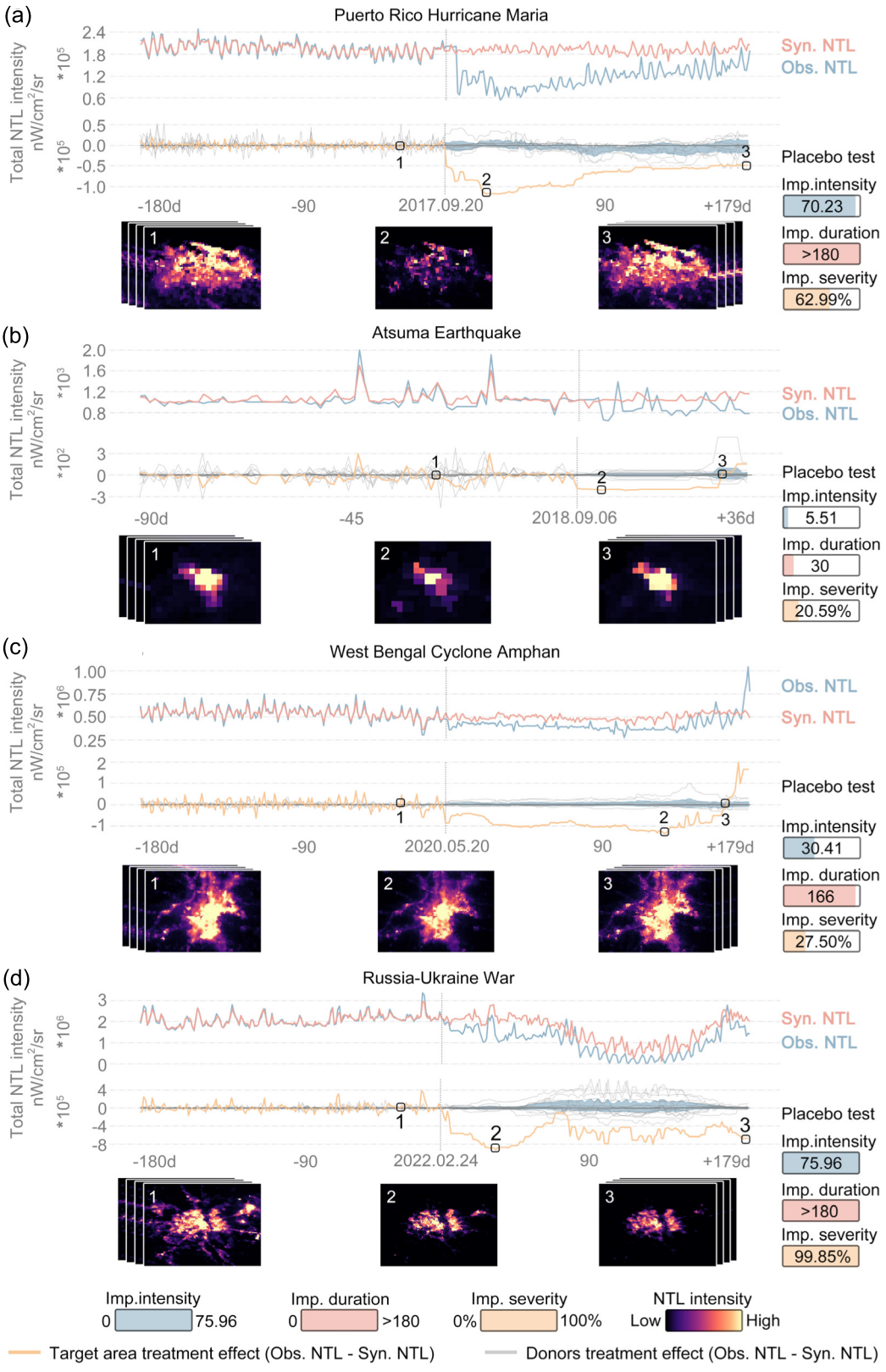

Fig. 5. Disaster impact assessment with results of RF-SC model, including synthetic NTL and observed NTL, treatment effects of the target area and donors (placebo test), three impact assessment metrics, and snapshots of NTL images at different dates before and after the disasters. The gray dashed line represents the disaster occurrence time. Four examples were presented: (a) Puerto Rico Hurricane Maria, (b) Atsuma Earthquake, (c) West Bengal Cyclone Amphan, and (d) Russia-Ukraine War. Assessments of other disasters are presented in Supplementary Fig. S1.

low-intensity disaster impacts was further validated through comparisons with other commonly used time series analysis models, such as BFAST and LSTM. We assessed BFAST's disaster detection capability by plotting trend components for

TABLE I
IMPACT ASSESSMENT METRICS OF EACH DISASTER

Regions and disasters	Impact duration (days)	Impact intensity	Impact severity
Ecuador Earthquake	13	0.12	1.65%
Valencia Flood	39	0.44	2.66%
Kochi Flood	12	0.45	7.90%
Petrinja Earthquake	10	0.49	5.07%
Florida Hurricane Irma	24	0.73	5.04%
Townsville Flood	27	0.97	5.94%
Hatay Earthquake	16	1.20	10.02%
Zhuhai Typhoon Hato	30	1.56	7.81%
Taizhou Typhoon Lekima	47	1.66	5.96%
Hubei Flood	42	3.63	11.86%
Chiapas Earthquake	69	4.06	21.55%
Atsuma Earthquake	30	5.51	20.59%
Khanh Hoa Typhoon Damrey	88	6.51	12.04%
North Carolina Hurricane Florence	84	7.35	14.62%
Mocoa Flood	57	11.12	31.67%
West Bengal Cyclone Amphan	166	30.41	27.50%
Azerbaijan-Armenia War	>180	40.85	45.67%
Syria Civil War	>180	55.55	46.83%
Puerto Rico Hurricane Maria	>180	70.23	62.99%
Russia-Ukraine War	>180	75.96	99.85%

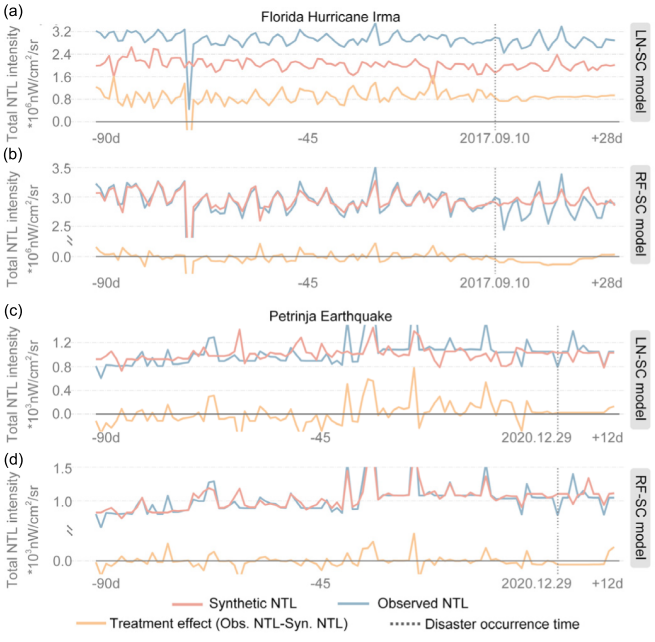

Fig. 6. Synthetic NTL, observed NTL, and treatment effect patterns generated by the LN-SC model and RF-SC model in (a) and (b) Florida Hurricane Irma, and (c) and (d) Petrinja Earthquake.

selected cases and marking breakpoints to visually inspect their alignment with disaster occurrences. Both our proposed RF-SC model and BFAST model successfully detected the impact of disasters with a high impact intensity, such as Puerto Rico Hurricane Maria (70.23; Fig. 7(b) and Table I) and Syria Civil War [55.55; Fig. 7(d)]. When it comes to disasters, however, with a relatively low disaster impact, such as the Kochi Flood (0.45) and Florida Hurricane Irma (0.73), the RF-SC model exhibited a stable and robust performance, while BFAST tended to under-detect the impact. For instance, two significant NTL changes were detected by BFAST but were 249 days and 93 days before and after the occurrence of Khanh Hoa Typhoon Damrey, respectively [Fig. 7(c)]. Similar under-detection was observed in Taizhou Typhoon Lekima [202 days before and 143 days after; Fig. 7(f)], Kochi Flood [155 days after; Fig. 7(a)], and Florida Hurricane Irma [not detected; Fig. 7(e)].

We calculated the Mean Absolute Percentage Error (MAPE) to compare the error in estimating post-disaster synthetic NTL time series between the RF-SC model and LSTM. 17 out of 20 studied disasters showed a lower post-disaster MAPE with the RF-SC model than with LSTM, further demonstrating better robustness of the RF-SC model in estimating BAU NTL time series. An exception was found in the Syria Civil War (7.10% versus 5.60%), Taizhou Typhoon Lekima (4.42% versus 2.94%), and Hubei Flood (3.96% versus 3.55%), where the MAPEs of RF-SC model were slightly higher than LSTM (Fig. 8(a) and (b); Table S4). The MAPE of the RF-SC model was, nevertheless, similarly minimal in these exceptions, thus not diluting our conclusion on the outperformance of RF-SC over LSTM. Besides, although LSTM yielded a perfectly fitting performance of pre-disaster NTL, it was most likely due

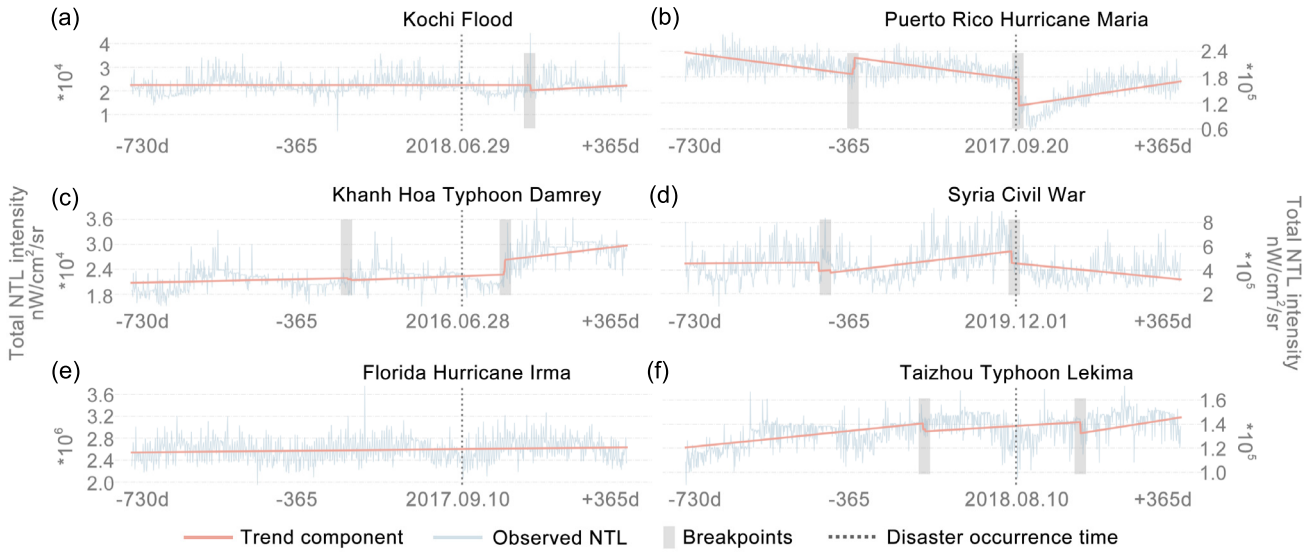

Fig. 7. BFAST trend component extracted from 1095 days preprocessed NTL of (a) Kochi Flood, (b) Puerto Rico Hurricane Maria, (c) Khanh Hoa Typhoon Damrey, (d) Syria Civil War, (e) Florida Hurricane Irma, and (f) Taizhou Typhoon Lekima.

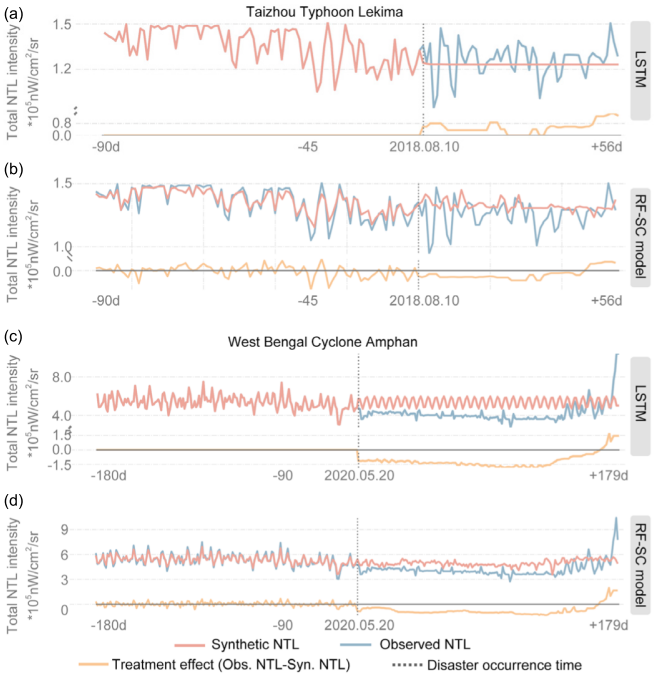

Fig. 8. Synthetic NTL, observed NTL, and treatment effect patterns generated by LSTM and RF-SC model in (a) and (b) Taizhou Typhoon Lekima, and (c) and (d) West Bengal Cyclone Amphan.

to overfitting as the post-disaster predicted NTL presented an abnormally stable trajectory [Fig. 8(a) and (c)].

V. Discussion

Constructing a reliable and robust BAU NTL time series is essential to unleashing the full potential of NTL-based disaster impact assessment and ensuring its effectiveness. Our proposed RF-SC model addressed the key drawbacks of time series modeling-based approaches. In spite of their widespread use, our analysis indicates that these approaches are susceptible to unexplained covarying factors, noise, and uncertainties that are not well-captured by time series models. Indeed, the high temporal variation, great variety of under-studied uncertainty sources, and complicated patterns make it hardly possible for any time series model to perfectly capture these items and reconstruct a reliable BAU NTL time series. As shown in our comparison analysis, without addressing these issues, the impact of disaster tends to be under-detected or buried in the high temporal variation of NTL data; moreover, the NTL time series pattern, comprising accounted and unaccounted factors, is highly region-specific, suggesting that using a one-size-fits-all time series model to construct BAU NTL time series is also unrealistic. Cross comparing existing studies on the same disaster, the estimated BAU NTL time series differ significantly across different time series models used (e.g., linear model, linear+harmonic model, exponential model, etc.) [17], [55]. In contrast, incorporating an SC model allows us to bypass modeling these unexplained uncertainties and isolate the disaster's impact from other covarying factors. These differences are mainly because time series modeling-based approaches only employ the historical time series of the target area for model fitting and BAU NTL estimation, while SC-based approaches (including our proposed RF-SC model) further use temporal information from areas sharing similar socioeconomic and environmental characteristics.

Our further investigation indicated that our proposed RF-SC model is less sensitive to model settings, such as the number of optimized donors and the type of covariates. Whether trained with 9 or 12 donors (out of an original 15) or without single-valued covariates (e.g., road length, building height), the model consistently exhibited high precision (Table S5). Besides, different viewing zenith angles (VZAs) of NTL images can lead to variations in NTL intensity (i.e., known as angular effect), which thereby might also bias our results [5]. We performed two additional analyses on the angular effect by comparing (i) the total NTL radiance and (ii) the detected treatment effect and impact assessment metrics, with and without correcting the angular effect (see Supplementary Text 4). Our analysis indicates that the angular effect has an ignorable

influence on our model and results. In addition, we smoothed the total NTL curve using a median filter when calculating the impact metrics and detecting the treatment effect, which would further attenuate the impact of VZA on our results.

Our analysis also underlined the necessity of the proposed RF-SC model framework, as well as its advantages over the conventional LN-SC model framework. Besides, our proposed DTW-based similarity measurement offered a quantitative and objective solution to select optimal donors and avoided the time-consuming trial-and-error method; hence, we make the entire methodological framework free of subjective and manual operation, thereby making it easier to generalize to wider applications. Besides, our further analysis also indicates that an optimized group of donors is necessary for constructing high-quality synthetic NTL and robust performance in disaster impact detection (see Supplementary Text 5).

RF-SC model and the resulting assessment metrics provide a timely and effective solution to obtain quantitative insights into disaster impact. It complements existing disaster assessment indicators adopted by the government, such as the number of people affected and economic losses [56], [57], which are often labor-intensive and time-consuming to obtain. Our methodology allows for the rapid, low-cost, and near-real-time tracking of disaster impact and progression on a global scale. Besides, NTL-based assessment contributes to a more comprehensive understanding of the impact of disasters from a socioeconomic perspective. In comparison, most of the other geospatial approaches mainly look into the physical impacts of disasters, such as flood area mapping and modeling [58], building damage detection [59], and electricity supply restoration estimation [60]. Understanding the socioeconomic impact of disasters is imperative as it usually lasts longer than the physical impact. For example, Hurricane Maria not only caused irreversible damage to electrical facilities and buildings but also had a profound impact on the population. Acosta et al. [61] reported a persistent and long-term population decrease of up to 35% in Puerto Rico, which further slowed down the socioeconomic recovery of Puerto Rico. Our further analysis showed that Puerto Rico only recovered to 82% of its BAU level of human activity 360 days after the disaster (Fig. S3). While geospatial data, like POIs, smartphone geolocation data [62], and social media records, have also been applied to quantify disaster impact, their applicability is more or less constrained by incomparability across time, space, and events, limited spatial and temporal availability, delayed response, and biased representation.

Finally, we highlight the following limitations of our study. First, our study was based on the total NTL intensity aggregated on a city scale or county scale rather than on a pixel basis. This is also true for other SC-based studies. This is mainly because of the high heterogeneity of contributing factors to NTL changes at a pixel scale. In other words, there are so many noncovarying factors that contribute to NTL changes of target and other pixels, making it challenging to identify suitable donors sharing similar characteristics. This limitation somehow constrains the spatial details achievable from SC-based approaches. Second, the daily NTL images were derived from the BRDF-corrected NTL radiance layer of the VNP46 product, which is subject to prevailing data gaps issues [33]. We estimated the NTL intensity of data gaps by polynomial interpolation. This operation was likely to underestimate the disaster severity, especially in the case when a succession of data gaps falls into the first few days of disaster occurrence. In spite of other available gap-filling algorithms, they are either computationally intensive or rely on other auxiliary data, which brings obstacles to rapid assessments [4], [63], [64]. Besides, our further analysis demonstrated that the choice of interpolation approach would not affect our assessment results. This finding is also corroborated by a previous study that showed imprecise measurements at pixel scale would not influence the detection of the difference between observed and synthetic outcome variables [65]. Third, the inherent issue of VIIRS NTL data—a less ideal overpass time (∼1:30 am)—also tends to underestimate the severity of disaster impact as a considerable proportion of outdoor lighting is turned off after midnight, compared with peaking lighting hours (7–10 pm) [66].

VI. Conclusion

NTL-based disaster assessment stands out from other assessment approaches due to its unique capability to provide a timely, long-term, and spatiotemporally consistent proxy of the socioeconomic response to disaster impacts. In this study, we used daily NTL images from NASA's Black Marble VIIRS product suite and extended before NTL-based disaster assessment approaches in BAU NTL estimation with an improved SC model (RF-SC model), which incorporated a DTW-based donor selection optimization and Random Forest Regression model. Applying our proposed RF-SC model, we generated a robust synthetic NTL time series as a counterfactual BAU NTL and assessed the impacts of 20 severe disasters across the world. Through a series of thorough evaluations and comparisons against existing approaches, we demonstrated the superior performance of our model in constructing reliable BAU and securing robust disaster impact detection, especially for disasters with short-term and low-intensity impacts. Besides, our assessments, together with the derived impact assessment metrics, offer comprehensive insights into the accumulative impact, severity, and duration of disasters, which help to reveal the differences in socioeconomic resilience across regions. To sum up, our study proposes a feasible framework to address the key drawbacks and better use the full potential of NTL-based disaster impact assessment. Our framework not only benefits regions lacking cost-effective tools for assessing disaster impact and post-disaster recovery but can also assist in quantitative evaluation of the progress toward goals and initiatives for disaster risk reduction (e.g., SDG Target 11.5 and Sendai Framework for Disaster Risk Reduction).

References

[1] C. D. Elvidge, K. E. Baugh, E. A. Kihn, H. W. Kroehl, E. R. Davis, and C. W. Davis, "Relation between satellite observed visible-near infrared emissions, population, economic activity and electric power consumption," *Int. J. Remote Sens.*, vol. 18, no. 6, pp. 1373–1379, Apr. 1997, doi: 10.1080/014311697218485.

[2] C. D. Elvidge, F. C. Hsu, M. Zhizhin, T. Ghosh, and T. Sparks, "Statistical moments of VIIRS night-time lights," *Int. J. Remote Sens.*, vol. 45, no. 21, pp. 7778–7802, Nov. 2024, doi: 10.1080/01431161.2022.2161857.

[3] M. M. Bennett and L. C. Smith, "Advances in using multitemporal night-time lights satellite imagery to detect, estimate, and monitor socioeconomic dynamics," *Remote Sens. Environ.*, vol. 192, pp. 176–197, Apr. 2017, doi: 10.1016/j.rse.2017.01.005.

[4] X. Tan and X. Zhu, "CRYSTAL: A novel and effective method to remove clouds in daily nighttime light images by synergizing spatiotemporal information," *Remote Sens. Environ.*, vol. 295, Sep. 2023, Art. no. 113658, doi: 10.1016/j.rse.2023.113658.

[5] X. Li et al., "Using radiant intensity to characterize the anisotropy of satellite-derived city light at night," *Remote Sens. Environ.*, vol. 271, Mar. 2022, Art. no. 112920, doi: 10.1016/j.rse.2022.112920.

[6] Z. Chen et al., "An extended time series (2000–2018) of global NPP-VIIRS-like nighttime light data from a cross-sensor calibration," *Earth Syst. Sci. Data*, vol. 13, no. 3, pp. 889–906, Mar. 2021, doi: 10.5194/essd-13-889-2021.

[7] B. Guo, D. Hu, and Q. Zheng, "Potentiality of SDGSAT-1 glimmer imagery to investigate the spatial variability in nighttime lights," *Int. J. Appl. Earth Observ. Geoinf.*, vol. 119, May 2023, Art. no. 103313, doi: 10.1016/j.jag.2023.103313.

[8] Q. Zheng, K. C. Seto, Y. Zhou, S. You, and Q. Weng, "Nighttime light remote sensing for urban applications: Progress, challenges, and prospects," *ISPRS J. Photogramm. Remote Sens.*, vol. 202, pp. 125–141, Aug. 2023, doi: 10.1016/j.isprsjprs.2023.05.028.

[9] M. Zhao et al., "Mapping urban dynamics (1992–2018) in Southeast Asia using consistent nighttime light data from DMSP and VIIRS," *Remote Sens. Environ.*, vol. 248, Oct. 2020, Art. no. 111980, doi: 10.1016/j.rse.2020.111980.

[10] J. F. Martinez, K. Macmanus, E. C. Stokes, Z. Wang, and A. de Sherbinin, "Suitability of NASA's black marble daily nighttime lights for population studies at varying spatial and temporal scales," *Remote Sens.*, vol. 15, no. 10, p. 2611, May 2023. [Online]. Available: https://www.mdpi.com/2072-4292/15/10/2611

[11] K. Shi et al., "Spatiotemporal variations of CO_2 emissions and their impact factors in China: A comparative analysis between the provincial and prefectural levels," *Appl. Energy*, vols. 233–234, pp. 170–181, Jan. 2019, doi: 10.1016/j.apenergy.2018.10.050.

[12] M. Kocifaj, S. Wallner, and J. C. Barentine, "Measuring and monitoring light pollution: Current approaches and challenges," *Science*, vol. 380, no. 6650, pp. 1121–1124, Jun. 2023, doi: 10.1126/science.adg0473.

[13] C. C. M. Kyba, Y. Ö. Altintaş, C. E. Walker, and M. Newhouse, "Citizen scientists report global rapid reductions in the visibility of stars from 2011 to 2022," *Science*, vol. 379, no. 6629, pp. 265–268, Jan. 2023, doi: 10.1126/science.abq7781.

[14] M. O. Román et al., "Satellite-based assessment of electricity restoration efforts in Puerto Rico after Hurricane Maria," *PLoS ONE*, vol. 14, no. 6, Jun. 2019, Art. no. e0218883, doi: 10.1371/journal.pone.0218883.

[15] J. Xu and Y. Qiang, "Spatial assessment of community resilience from 2012 Hurricane Sandy using nighttime light," *Remote Sens.*, vol. 13, no. 20, p. 4128, Oct. 2021. [Online]. Available: https://www.mdpi.com/2072-4292/13/20/4128

[16] X. Li, F. Chen, and X. Chen, "Satellite-observed nighttime light variation as evidence for global armed conflicts," *IEEE J. Sel. Topics Appl. Earth Observ. Remote Sens.*, vol. 6, no. 5, pp. 2302–2315, Oct. 2013, doi: 10.1109/JSTARS.2013.2241021.

[17] Z. Zheng et al., "Estimates of power shortages and affected populations during the initial period of the Ukrainian–Russian conflict," *Remote Sens.*, vol. 14, no. 19, p. 4793, Sep. 2022, doi: 10.3390/rs14194793.

[18] W. Jiang, G. He, T. Long, and H. Liu, "Ongoing conflict makes Yemen dark: From the perspective of nighttime light," *Remote Sens.*, vol. 9, no. 8, p. 798, Aug. 2017. [Online]. Available: https://www.mdpi.com/2072-4292/9/8/798

[19] UNDRR. (2024). *Sendai Framework for Disaster Risk Reduction 2015–2030 | UNDRR*. Accessed: Sep. 4, 2024. [Online]. Available: https://www.undrr.org/publication/sendai-framework-disaster-risk-reduction-2015-2030

[20] UN. *Goal 11 | Department of Economic and Social Affairs*. Accessed: Sep. 4, 2024. [Online]. Available: https://sdgs.un.org/goals/goal11#targets_and_indicators

[21] S. Gao, Y. Chen, L. Liang, and A. Gong, "Post-earthquake night-time light piecewise (PNLP) pattern based on NPP/VIIRS night-time light data: A case study of the 2015 Nepal earthquake," *Remote Sens.*, vol. 12, no. 12, p. 2009, Jun. 2020, doi: 10.3390/rs12122009.

[22] Y. Yuan et al., "The changes in nighttime lights caused by the Turkey–Syria earthquake using NOAA-20VIIRS day/night band data," *Remote Sens.*, vol. 15, no. 13, p. 3438, Jul. 2023. [Online]. Available: https://www.mdpi.com/2072-4292/15/13/3438

[23] J. Xu, Y. Qiang, H. Cai, and L. Zou, "Power outage and environmental justice in winter storm uri: An analytical workflow based on nighttime light remote sensing," *Int. J. Digit. Earth*, vol. 16, no. 1, pp. 2259–2278, Oct. 2023, doi: 10.1080/17538947.2023.2224087.

[24] Y. Qiang, Q. Huang, and J. Xu, "Observing community resilience from space: Using nighttime lights to model economic disturbance and recovery pattern in natural disaster," *Sustain. Cities Soc.*, vol. 57, Jun. 2020, Art. no. 102115.

[25] A. Kwasinski, F. Andrade, M. J. Castro-Sitiriche, and E. O'Neill-Carrillo, "Hurricane Maria effects on Puerto Rico electric power infrastructure," *IEEE Power Energy Technol. Syst. J.*, vol. 6, no. 1, pp. 85–94, Mar. 2019, doi: 10.1109/JPETS.2019.2900293.

[26] F. Li, Q. Wang, W. Hu, J. Liu, and X. Zhang, "Rapid assessment of disaster damage and economic resilience in relation to the flooding in Zhengzhou, China in 2021," *Remote Sens. Lett.*, vol. 13, no. 7, pp. 651–662, Jul. 2022, doi: 10.1080/2150704x.2022.2068987.

[27] Z. Wang, M. O. Román, V. L. Kalb, S. D. Miller, J. Zhang, and R. M. Shrestha, "Quantifying uncertainties in nighttime light retrievals from suomi-NPP and NOAA-20VIIRS day/night band data," *Remote Sens. Environ.*, vol. 263, Sep. 2021, Art. no. 112557, doi: 10.1016/j.rse.2021.112557.

[28] A. S. de Miguel, C. C. M. Kyba, J. Zamorano, J. Gallego, and K. J. Gaston, "The nature of the diffuse light near cities detected in nighttime satellite imagery," *Sci. Rep.*, vol. 10, no. 1, p. 7829, May 2020, doi: 10.1038/s41598-020-64673-2.

[29] X. Zhao et al., "NPP-VIIRS DNB daily data in natural disaster assessment: Evidence from selected case studies," *Remote Sens.*, vol. 10, no. 10, p. 1526, Sep. 2018. [Online]. Available: https://www.mdpi.com/2072-4292/10/10/1526

[30] B. Dong et al., "Identifying and classifying shrinking cities using long-term continuous night-time light time series," *Remote Sens.*, vol. 13, no. 16, p. 3142, Aug. 2021. [Online]. Available: https://www.mdpi.com/2072-4292/13/16/3142

[31] CU EM-DAT. (2024). *The International Disaster Database*. Accessed: May 24, 2024. [Online]. Available: https://www.emdat.be/

[32] M. O. Román et al., "NASA's black marble nighttime lights product suite," *Remote Sens. Environ.*, vol. 210, pp. 113–143, Jun. 2018, doi: 10.1016/j.rse.2018.03.017.

[33] Q. Zheng, Q. Weng, Y. Zhou, and B. Dong, "Impact of temporal compositing on nighttime light data and its applications," *Remote Sens. Environ.*, vol. 274, Jun. 2022, Art. no. 113016, doi: 10.1016/j.rse.2022.113016.

[34] N. Gorelick, M. Hancher, M. Dixon, S. Ilyushchenko, D. Thau, and R. Moore, "Google Earth Engine: Planetary-scale geospatial analysis for everyone," *Remote Sens. Environ.*, vol. 202, pp. 18–27, Dec. 2017, doi: 10.1016/j.rse.2017.06.031.

[35] F. Serra-Burriel, P. Delicado, A. T. Prata, and F. M. Cucchietti, "Estimating heterogeneous wildfire effects using synthetic controls and satellite remote sensing," *Remote Sens. Environ.*, vol. 265, Nov. 2021, Art. no. 112649, doi: 10.1016/j.rse.2021.112649.

[36] Y. Xu, "Generalized synthetic control method: Causal inference with interactive fixed effects models," *Political Anal.*, vol. 25, no. 1, pp. 57–76, Jan. 2017.

[37] A. Abadie, "Using synthetic controls: Feasibility, data requirements, and methodological aspects," *J. Econ. Literature*, vol. 59, no. 2, pp. 391–425, Jun. 2021, doi: 10.1257/jel.20191450.

[38] S. Marinello, J. Leider, O. Pugach, and L. M. Powell, "The impact of the Philadelphia beverage tax on employment: A synthetic control analysis," *Econ. Hum. Biol.*, vol. 40, Jan. 2021, Art. no. 100939, doi: 10.1016/j.ehb.2020.100939.

[39] V. Geloso and J. B. Pavlik, "The Cuban revolution and infant mortality: A synthetic control approach," *Explor. Econ. Hist.*, vol. 80, Apr. 2021, Art. no. 101376, doi: 10.1016/j.eeh.2020.101376.

[40] T. A. P. West et al., "Action needed to make carbon offsets from forest conservation work for climate change mitigation," *Science*, vol. 381, no. 6660, pp. 873–877, Aug. 2023, doi: 10.1126/science.ade3535.

[41] R. Hang, Q. Liu, H. Song, Y. Sun, F. Zhu, and H. Pei, "Graph regularized nonlinear ridge regression for remote sensing data analysis," *IEEE J. Sel. Topics Appl. Earth Observ. Remote Sens.*, vol. 10, no. 1, pp. 277–285, Jan. 2017, doi: 10.1109/JSTARS.2016.2574802.

[42] G. Zhao, Z. Li, and M. Yang, "Comparison of twelve machine learning regression methods for spatial decomposition of demographic data using multisource geospatial data: An experiment in Guangzhou City, China," *Appl. Sci.*, vol. 11, no. 20, p. 9424, Oct. 2021. [Online]. Available: https://www.mdpi.com/2076-3417/11/20/9424

[43] M. Belgiu and O. Csillik, "Sentinel-2 cropland mapping using pixel-based and object-based time-weighted dynamic time warping analysis," *Remote Sens. Environ.*, vol. 204, pp. 509–523, Jan. 2018, doi: 10.1016/j.rse.2017.10.005.

[44] W.-C. Wang, K.-W. Chau, L. Qiu, and Y.-B. Chen, "Improving forecasting accuracy of medium and long-term runoff using artificial neural network based on EEMD decomposition," *Environ. Res.*, vol. 139, pp. 46–54, May 2015, doi: 10.1016/j.envres.2015.02.002.

[45] P. O. Gislason, J. A. Benediktsson, and J. R. Sveinsson, "Random forests for land cover classification," *Pattern Recognit. Lett.*, vol. 27, no. 4, pp. 294–300, Mar. 2006, doi: 10.1016/j.patrec.2005.08.011.

[46] J. Verbesselt, R. Hyndman, G. Newnham, and D. Culvenor, "Detecting trend and seasonal changes in satellite image time series," *Remote Sens. Environ.*, vol. 114, no. 1, pp. 106–115, Jan. 2010, doi: 10.1016/j.rse.2009.08.014.

[47] Y. Yu, X. Si, C. Hu, and J. Zhang, "A review of recurrent neural networks: LSTM cells and network architectures," *Neural Comput.*, vol. 31, no. 7, pp. 1235–1270, Jul. 2019, doi: 10.1162/neco_a_01199.

[48] S. Hochreiter and J. Schmidhuber, "Long short-term memory," *Neural Comput.*, vol. 9, no. 8, pp. 1735–1780, 1997, doi: 10.1162/neco.1997.9.8.1735.

[49] T. A. P. West, J. Börner, E. O. Sills, and A. Kontoleon, "Overstated carbon emission reductions from voluntary REDD+ projects in the Brazilian Amazon," *Proc. Nat. Acad. Sci. USA*, vol. 117, no. 39, pp. 24188–24194, Sep. 2020, doi: 10.1073/pnas.2004334117.

[50] M. Zahn. (2024). *Puerto Rico's Power Grid is Struggling 5 Years After Hurricane Maria. Here's Why*. Accessed: Jul. 1, 2024. [Online]. Available: https://abcnews.go.com/Technology/puerto-ricos-power-grid-struggling-years-hurricane-maria/story?id=90151141

[51] J. Abbasi, "Hurricane Maria and Puerto Rico: A physician looks back at the storm," *JAMA*, vol. 320, no. 7, pp. 629–630, Aug. 2018, doi: 10.1001/jama.2018.8244.

[52] D. Zhang, H. Huang, N. Roy, M. M. Roozbahani, and J. D. Frost, "Black marble nighttime light data for disaster damage assessment," *Remote Sens.*, vol. 15, no. 17, p. 4257, Aug. 2023, doi: 10.3390/rs15174257.

[53] X. Fan, G. Nie, Y. Deng, J. An, J. Zhou, and H. Li, "Rapid detection of earthquake damage areas using VIIRS nearly constant contrast nighttime light data," *Int. J. Remote Sens.*, vol. 40, nos. 5–6, pp. 2386–2409, Mar. 2019, doi: 10.1080/01431161.2018.1460512.

[54] L. Wang, H. Lei, and H. Xu, "Analysis of nighttime light changes and trends in the 1-year anniversary of the Russia–Ukraine conflict," *IEEE J. Sel. Topics Appl. Earth Observ. Remote Sens.*, vol. 17, pp. 4084–4099, 2024, doi: 10.1109/JSTARS.2024.3357727.

[55] C. Huang et al., "Mapping of nighttime light trends and refugee population changes in Ukraine during the Russian–Ukrainian war," *Frontiers Environ. Sci.*, vol. 11, Jan. 2023, Art. no. 1055100, doi: 10.3389/fenvs.2023.1055100.

[56] FEMA. *What is Hazus?* Accessed: Sep. 4, 2024. [Online]. Available: https://www.fema.gov/zh-hans/flood-maps/tools-resources/flood-map-products/hazus/about

[57] Z. Li. *2024 Nian Shangbannian Quanguo Ziran Zaihai Qingkuang*. Accessed: Sep. 4, 2024. [Online]. Available: https://www.mem.gov.cn/xw/yjglbgzdt/202407/t20240712_494600.shtml

[58] B. F. Sanders et al., "Large and inequitable flood risks in Los Angeles, California," *Nature Sustainability*, vol. 6, no. 1, pp. 47–57, Oct. 2022, doi: 10.1038/s41893-022-00977-7.

[59] L. Dong and J. Shan, "A comprehensive review of earthquake-induced building damage detection with remote sensing techniques," *ISPRS J. Photogramm. Remote Sens.*, vol. 84, pp. 85–99, Oct. 2013.

[60] C. Brelsford et al., "A dataset of recorded electricity outages by United States county 2014–2022," *Sci. Data*, vol. 11, no. 1, p. 271, Mar. 2024, doi: 10.1038/s41597-024-03095-5.

[61] R. J. Acosta, N. Kishore, R. A. Irizarry, and C. O. Buckee, "Quantifying the dynamics of migration after hurricane Maria in Puerto Rico," *Proc. Nat. Acad. Sci. USA*, vol. 117, no. 51, pp. 32772–32778, Dec. 2020, doi: 10.1073/pnas.2001671117.

[62] B. Hong, B. J. Bonczak, A. Gupta, and C. E. Kontokosta, "Measuring inequality in community resilience to natural disasters using large-scale mobility data," *Nature Commun.*, vol. 12, no. 1, p. 1870, Mar. 2021, doi: 10.1038/s41467-021-22160-w.

[63] Y. Hu, X. Zhou, D. Yamazaki, and J. Chen, "A self-adjusting method to generate daily consistent nighttime light data for the detection of short-term rapid human activities," *Remote Sens. Environ.*, vol. 304, Apr. 2024, Art. no. 114077, doi: 10.1016/j.rse.2024.114077.

[64] Y. Ye et al., "Modeling and prediction of NPP-VIIRS nighttime light imagery based on spatiotemporal statistical method," *IEEE Trans. Geosci. Remote Sens.*, vol. 59, no. 6, pp. 4934–4946, Jun. 2021, doi: 10.1109/TGRS.2020.3011695.

[65] G. Demarchi, J. Subervie, T. Catry, and I. Tritsch, "Using publicly available remote sensing products to evaluate REDD+ projects in Brazil," *Global Environ. Change*, vol. 80, May 2023, Art. no. 102653, doi: 10.1016/j.gloenvcha.2023.102653.

[66] T. Nachtlichter et al., "What's in a Watt? Interpreting nightlights satellite data via citizen science observations," Res. Square, GFZ German Res. Centre Geosci., Potsdam, Germany, Version 1, Aug. 2024, doi: 10.21203/rs.3.rs-4743740/v1.

Te Mu received the B.A. degree in history from Shanxi University, Taiyuan, China, in 2018, and the M.Arch. degree in architecture from Zhejiang University, Hangzhou, China, in 2023. He is currently pursuing the Ph.D. degree with the Department of Geography and Resource Management, The Chinese University of Hong Kong, Hong Kong, SAR, China.

His research interests include nighttime light remote sensing, disaster impact assessment, and remote sensing of urban environments.

Qiming Zheng received the Ph.D. degree from Zhejiang University, Hangzhou, China, in 2020.

He is currently an Assistant Professor with the Department of Geography and Resource Management, The Chinese University of Hong Kong, Hong Kong, SAR, China. His research centers on using geospatial techniques, environment and earth system models, and GeoAI approaches to address cutting-edge challenges in global environmental changes, urban sustainability, and climate change mitigation.

Sylvia Y. He received the B.S. degree in geography (concentration: GIS) from Sun Yat-sen University, Guangzhou, China, in 2003, the M.A. degree in geography from McMaster University, Hamilton, Canada, in 2006, and the Ph.D. degree in policy, planning, and development from the School of Public Policy, University of Southern California, Los Angeles, CA, USA, in 2012.

She is currently a Professor at the Department of Geography and Resource Management, The Chinese University of Hong Kong, Hong Kong, SAR, China. Her research interests include urban planning, transport planning and policy, travel behavior, spatial analysis, and urban analytics.